Rheological Properties and Small-Angle Neutron Scattering of a Shear Thickening, Nanoparticle Dispersion at High Shear Rates

Young S. Lee and Norman J. Wagner*

Department of Chemical Engineering and Center for Composite Materials, University of Delaware, Newark, Delaware 19716

The rheological properties and flow microstructure of a stable dispersion of spherical nanoparticles ($d = 32$ nm) are investigated and compared to the behavior of colloidal dispersions. The shear rheology and flow−small-angle neutron scattering of charge-stabilized silica nanoparticles dispersed in ethylene glycol are reported as a function of shear stress and particle volume fraction. A custom-built high-shear cone is employed to reach shear rates in excess of 10^4 s^{-1} in order to study shear thickening. The results are compared to previous model system studies on colloidal dispersions and to micromechanical models that relate the physical parameters of the system to the rheological response. Reversible shear thickening is observed at very high shear rates, and the measured transition stresses for shear thickening compare well to theoretical predictions for colloidal dispersions. Flow−small-angle neutron scattering measurements both in the radial and tangential orientations show a shear-induced structure near the shear thickening transition that is consistent with the hydrocluster mechanism of reversible shear thickening operative in colloidal dispersions. Hence, continuum fluid mechanics, and, in particular, lubrication hydrodynamics, is confirmed to be operative in the nanometer-scale gaps between the nanoparticle surfaces.

I. Introduction

There is fundamental interest in the use of nanoparticles for numerous industrial applications including faster, smarter, and more convenient communication components and devices.[1] It is well-established that dispersions of particles from micrometers in size down to particles of the order of ∼100 nm have been observed to undergo a transition to a shear-thickened state at appropriately high-shear stresses.[2−11] Shear thickening is marked by an increasing viscosity with increasing shear rate or shear stress. Of interest here is *reversible* shear thickening, as opposed to shear-induced aggregation. Although the shear thickening phenomenon can damage processing equipment and, therefore, is generally to be avoided, there are practical applications using shear thickening fluids such as damping and control devices,[12,13] electrorheology,[14] and personal body armor.[15,16] Lee and co-workers have shown that the ballistic performance of Kevlar fabrics can be improved by impregnating the fabrics with shear thickening fluid.

The rheology and shear-induced microstructure of shear thickening colloidal dispersions have been investigated using rheooptics[10,17] and small-angle neutron scattering.[5,6,9,18,19] Although shear thickening can now be predicted for many dispersions, the lower limit of particle size whereby reversible shear thickening can be observed has not been established. Watanabe and co-workers[19] demonstrated shear thickening in 80 nm diameter particle dispersion, and Maranzano and Wagner[5] also demonstrated that hydrocluster formation accompanies the shear thickening transition for 75 nm diameter particle dispersion using flow−small-angle neutron scattering (flow−SANS). This mechanism of reversible shear thickening necessitates that particles interact via short-range lubrication forces,[2,3,20] where the range of these forces is small relative to the particle size. Studying nanosized particle dispersion rheology probes interparticle spacing on the nanometer length scales.[21,22] It is therefore not evident a priori that similar mechanisms operate in nanoparticle dispersions, as the lubrication hydrodynamics will be significant only at length scales where the atomic structure of the suspending medium may become relevant. Recent research has shown surface roughness affects shear thickening,[23] and as surface roughness can be relatively larger for nanoparticles, the effect on shear thickening may be more significant for nanoparticles as compared to colloids. Thus, the following question can be posed: To what lower length scale does continuum hydrodynamics work when modeling colloidal dispersion rheology? We hypothesize that if continuum hydrodynamics holds for nanosized colloidal particles, then reversible shear thickening will be observed in concentrated dispersions of nanosized colloidal particles, albeit at very high shear rates or stresses, and that the onset of shear thickening should be predicted from theories and models developed to predict reversible shear thickening in concentrated colloidal dispersions.

One of the most important and dramatic manifestations of continuum hydrodynamics is lubrication hydrodynamics, which is responsible for the divergence of the force required to bring two particles together at constant velocity, i.e., the diverging force resulting from squeezing fluid from between two smooth, solid surfaces.[24,25] This force is responsible for mechanical phenomena of technological importance, including the formation of hydroclusters and shear thickening in concentrated colloidal dispersions. There are ample reports in the literature showing a breakdown of continuum hydrodynamics as the gap between macroscopic surfaces approach atomic scales.[21,26] Recently Mackay and co-workers[27] report a violation of continuum hydrodynamics for polystyrene nanoparticles dispersed in polystyrene. The violation of the Einstein equation is apparent when the interparticle spacing approaches the radius of gyration of the polymer "solvent", leading to a reduction in overall viscosity. However, there is no direct evidence that this breakdown in continuum hydrodynamic affects the dynamics of nanoparticle dispersions in Newtonian solvents.

In this paper we investigate the microstructure and rheology of stable, nanoparticle dispersions (charge stabilized) at high

* To whom correspondence should be addressed. E-mail: wagner@che.udel.edu.

10.1021/ie0512690 CCC: $33.50
Published on Web 06/28/2006

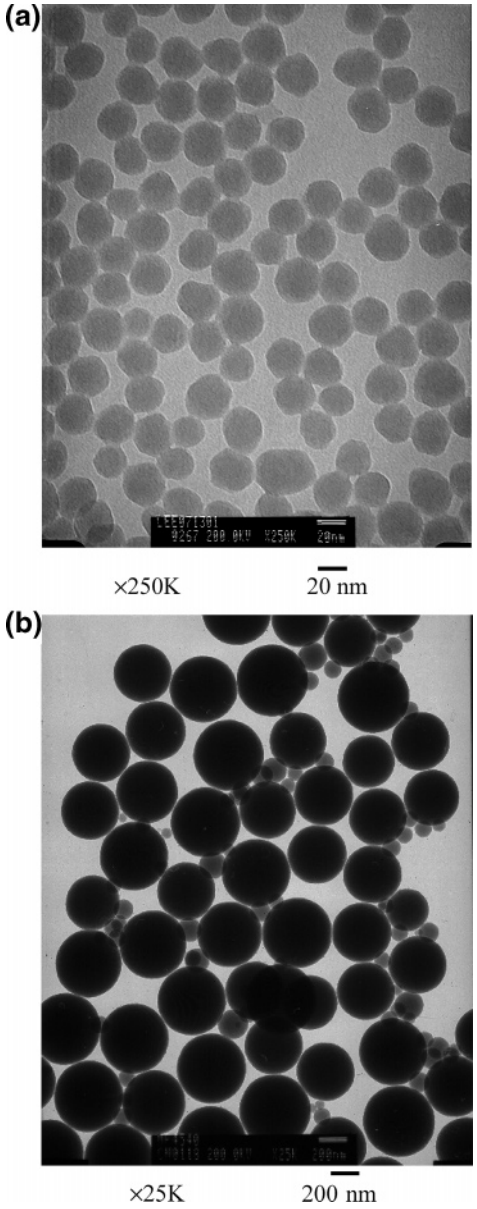

Figure 1. TEM photographs at magnification of (a) 250 000 for 32 nm particle dispersion and (b) 25 000 for 446 nm particle dispersion.

volume fractions and compare them with similar results for a colloidal dispersion comprised of particles an order of magnitude larger in size. A model dispersion of stable, silica nanoparticles in a viscous, Newtonian solvent (ethylene glycol) is studied using rotational rheometry and a custom-made, high shear rate cone and (flow−SANS).

II. Materials and Methods

A. Materials. The nanoparticle silica investigated here was obtained from Clariant (HIGHLINK OG 1-32), which is provided as an ethylene glycol (EG) based dispersion with a particle concentration of about 35 wt %. For comparison, 450 nm colloidal silica dispersions were obtained from Nissan Chemical (MP4540), which is provided as an aqueous dispersion with a particle concentration of about 40 wt %. The particle size distribution has been characterized with dynamic light scattering (DLS) (Brookhaven Particle Size Analyzer) and transmission electron microscope (TEM). Parts a and b of Figure 1 show transmission electron micrographs of the particles. The larger particle dispersion (Nissan) is observed to be slightly

Table 1. Characterization of Particles Studied in This Work

	HILINK OG 1-32	MP4540
supplier	Clariant	Nissan Chemical Co.
original base medium	ethylene glycol	water
d_{DLS} (diameter of particle)	32 ± 3.0	446 ± 8.4
d_{TEM} (diameter of particle)	31 ± 1.5	433 ± 3.6
ζ-potential (mV)	−28	−50
ρ_p (g/cm^3)	2.20	2.02

bimodal and contains a minor fraction of smaller particles. The average particle diameter (DLS, *z*-average) was determined to be 32 ± 3 nm for the Clariant nanoparticles and 446 ± 8.4 nm for the Nissan colloids. These values are consistent with the number average sizes determined by TEM measurements (see Table 1). Figure 2 shows the particle size distribution (PSD) histogram obtained from TEM image and image analyzing software. The ζ potentials have been determined in deionized water to be 28 mV for the Clariant nanoparticles and −50 mV for the Nissan colloids from electrophoresis (Brookhaven Zeta PALS, Table 1). Particle density was measured with a solution density meter (Anton Paar, Model DMA 48). Ideal mixing was assumed to relate the dispersion density (ρ_s) to that of the particles (ρ_p), and medium (ρ_m), with x being the weight fraction of particles,

$$\frac{1}{\rho_s} = \left(\frac{1}{\rho_p} - \frac{1}{\rho_m}\right)x + \frac{1}{\rho_m} \tag{1}$$

Figure 3 shows the measured density for varying weight fraction of silica (x), which fits the linear form suggested by eq 1. The

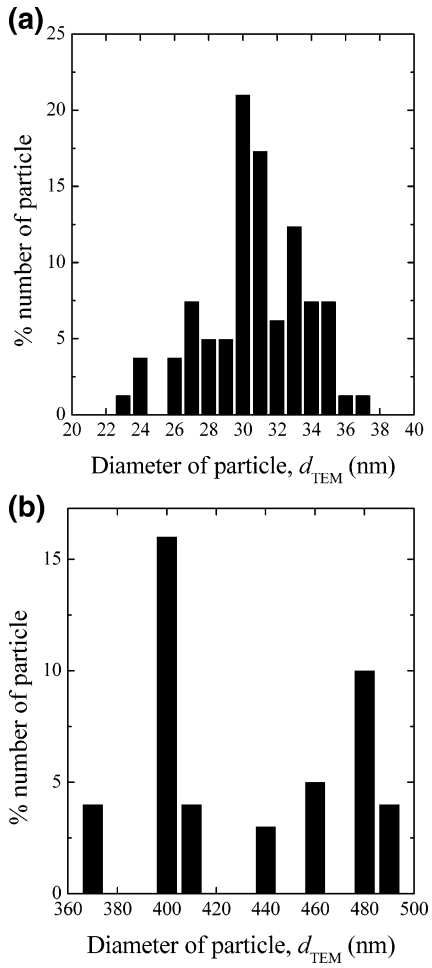

Figure 2. Particle size distribution histogram for (a) 32 nm particle and (b) 446 nm particle obtained from TEM measurements.

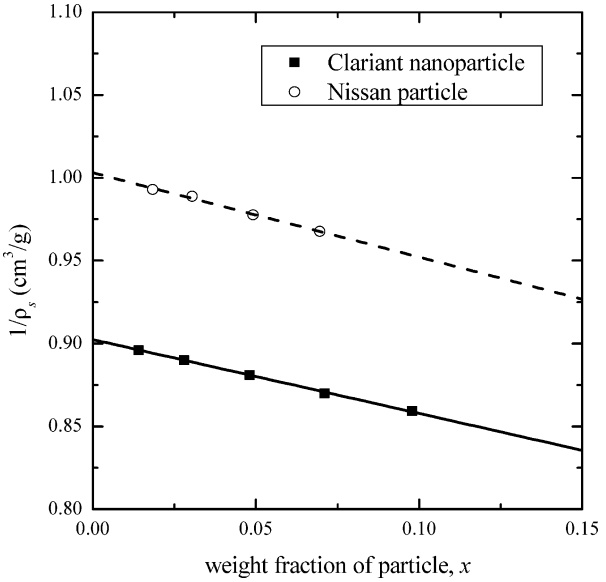

Figure 3. Density of the Clariant nanoparticles dispersed in EG (-■-) and the Nissan particles dispersed in water (-○-) as a function of particle weight fraction.

nanoparticle density $\rho_p = 2.20$ g/cm^3 is higher than the density of the Nissan colloids (2.02 g/cm^3, Table 1).

Dispersions of nanoparticles were prepared as follows. The original dispersion was concentrated using ultracentrifugation. The sediment was resuspended using a vortex mixer after adding a small amount of the supernatant liquid. Dilution with the supernatant liquor provided a series of silica nanoparticle dispersions in EG with known concentration and consistent medium properties.

For comparison, a dispersion of colloidal particles of 446 nm (Nissan Chemical Co.) was prepared. The suspending aqueous fluid was replaced with EG by repeated centrifugation followed by redispersion using a vortex mixer, four times. Both the nanoparticle and colloidal dispersion were redispersed as primary particles.

B. Rheological Measurements. For the Nissan colloidal silica dispersions, the steady shear experiments for a dispersion of silica particle of 446 nm were performed in a stress-controlled rheometer (SR-500, Rheometric Scientific) at 25 °C with a standard cone-plate geometry having a cone angle of 0.1 rad and a diameter of 25 mm. For the nanoparticle dispersions, rheological measurements were performed with a custom-built cone with a very low cone angle (Rheometric) in the controlled strain rheometer (ARES, TA Instruments). The fixture geometry is 50 mm diameter, 0.0023 rad angle, and 0.0068 mm of gap between truncation cone and plate. The performance of this tooling was checked with a Cannon certified viscosity standard S60 (0.102 Pa·s at 25 °C) and compared with measurements using a standard 50 mm cone with 0.0402 rad cone angle and 0.0483 mm gap. All measurement has been performed at 25 °C with a Peltier temperature control system.

Figure 4 shows the performance of the tooling at steady shear rates when measuring the viscosity of standard S60. The viscosity measured with the high shear cone is slightly higher than that measured with the standard cone, which agrees well with the reported standard viscosity. This viscosity offset may be a consequence of the difficulty in setting the miniscule gap in the low-angle cone. The temperature is also reported during steady shear flow. As shown in Figure 4 there is a small increase in temperature for shear rates above 10^{-4} s^{-1} because of viscous heating; however, the difference between set value and measured temperature is less than 0.5 °C at the highest shear rates ($\sim 10^5$ s^{-1}).

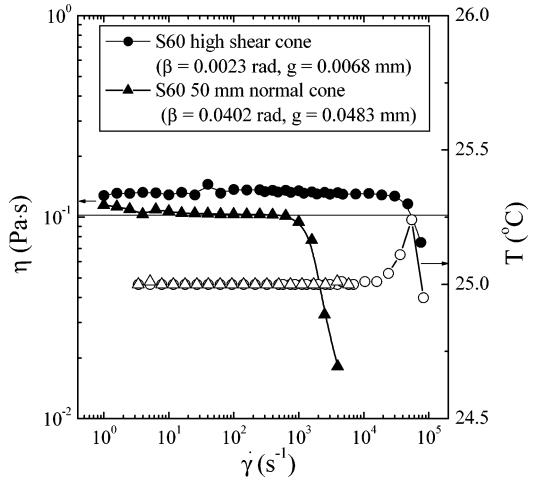

Figure 4. Steady shear viscosity (closed symbols) and temperature (open symbols) of standard oil (S60, $\eta = 0.102$ Pa·s) using 25 mm, 0.1 rad cone, and high shear cone at 25 °C with ARES rheometer. The line is the standard viscosity.

For dilute dispersions the viscosity was measured using a rolling ball viscometer (Anton Paar, automated micro viscometer) using different sliding angles. For reference, the viscosity of the medium (ethylene glycol) was found to be 16 ± 0.6 mPa·s at 25 °C.

C. Flow−Small-Angle Neutron Scattering. The flow−SANS measurements under shear flow were performed on the NG3 beamline at the National Center for Neutron Research (NCNR) at the National Institute of Standards and Technology (NIST) in Gaithersburg, MD, with a mean neutron wavelength of 6 Å and at detector distance of 12 m. The neutrons were directed through the sample which was contained in a Coutte shear cell (o.d. = 59 mm; i.d. = 61 mm). This experimental setup for flow−SANS has been discussed previously.[28]

The scattering profile under quiescent condition was obtained in the radial and tangential configurations at shear rates from 1 to 5000 s^{-1}. The scattering intensity $I(q)$ was measured as a function of the scattering vector $\mathbf{q}$, where $q = 4\pi/\lambda \sin(\theta/2)$ with θ being the scattering angle. The incident beam was in the direction of the velocity gradient, and the SANS profile was detected in a velocity−vorticity plane for radial (on-axis) configuration. For tangential (off-axis) configuration, the incident beam was in the direction of the velocity, and the SANS profile was detected in a velocity gradient−vorticity plane. The measured intensity was reduced with the scattering result from empty beam and empty cell according to NIST standard protocols with all of the standard corrections.

III. Results and Discussion

A. Rheological Behavior. Figure 5 shows the steady shear viscosity as a function of shear rate (a) and shear stress (b) of the 32 nm nanoparticle dispersions with different particle volume fractions at 25 °C measured with the high shear cone with the ARES rheometer. At low shear rate or shear stress, Newtonian plateaus are evident for all colloidal dispersions up to 44.7 vol %. Even at the highest concentration ($\phi = 0.486$), the viscosity at low shear rates appears to converge toward a Newtonian plateau. Significant shear thinning is observed, followed by weak shear thickening for samples with $\phi \geq 0.307$. These flow curves were observed to be reversible and reproducible. Experiments at the highest shear rates were limited by the sample ejecting

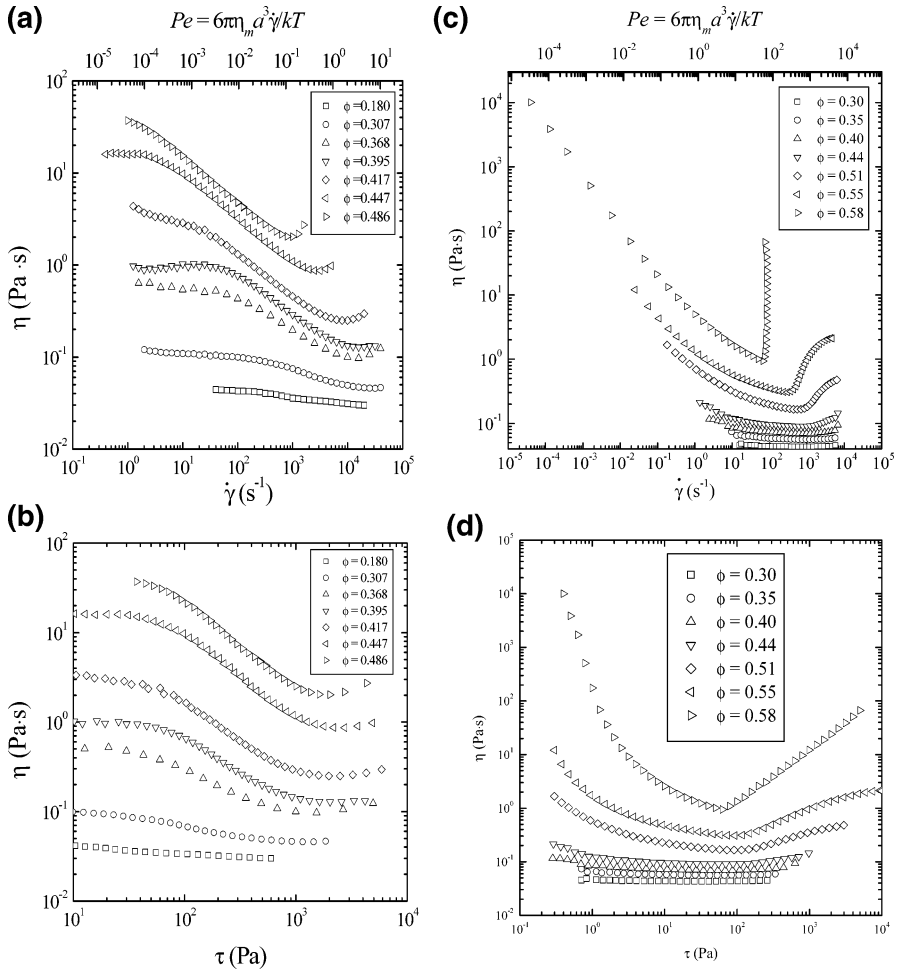

Figure 5. Steady shear viscosity curves measured with cone and plate geometry on (a, b) a ARES controlled rate rheometer for the dispersion of 32 nm silica particle dispersed in ethylene glycol and (c, d) a SR-500 controlled stress rheometer for the dispersion of 446 nm silica particle dispersed in ethylene glycol.

from the gap of the tooling, which is characteristic of shear thickening dispersions at high rotational speeds. However, it is apparent that the nanoparticle dispersions exhibit rheology typical of concentrated colloidal dispersions, including continuous shear thickening. For reference, the corresponding data for the 446 nm colloidal dispersions are shown in Figure 5c,d. Pronounced shear thickening is evident at a comparable volume fraction, but the shear thinning is shifted to lower shear rates relative to the nanoparticle dispersion, as expected. The corresponding Peclet numbers ($Pe = 6\pi\eta_m a^3\dot{\gamma}/k_B T$) are shown for reference in Figure 5a,c. When plotted versus Peclet number, it is apparent that the shear thinning occurs at comparable dimensionless shear rates despite the large difference in particle size. However, the onset of shear thickening does not scale with the Peclet number, which is a consequence of the role of electrostatic forces in hindering hydrocluster formation, as has been shown previously by experiment and theory.[3,4]

Having established behavior qualitatively similar to stable colloidal dispersions, it is relevant to determine if these nanoparticle dispersions follow the scaling behavior typical for colloidal dispersions. For concentrated colloidal dispersions in the absence of shear thickening, the relative dispersion viscosity approximates an empirical equation known as the Cross model;[29−31]

$$\eta_r = \eta_{r\infty} + \left(\frac{\eta_{r0} - \eta_{r\infty}}{1 + (b\tau_r)^m}\right) \qquad (2)$$

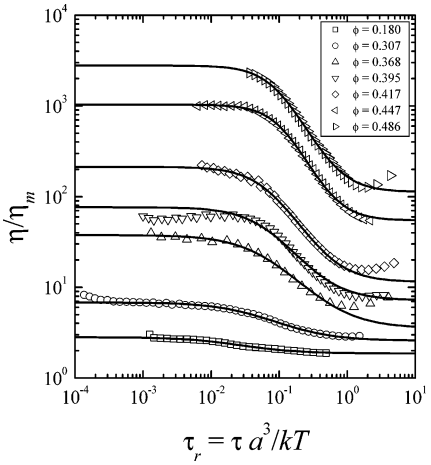

Figure 6. Cross model fits for the relative viscosity of 32 nm nanoparticle dispersions as a function of the reduced stress with different particle volume fraction.

with the reduced stress defined as $\tau_r = \tau a^3/kT$, $\eta_{r\infty}$ is the high shear rate-limiting viscosity, η_{r0} is the low shear rate-limiting viscosity, and b and m are fitting parameters.

As shown in Figure 6, the flow curves for nanoparticle dispersions show shear thickening behavior at high shear rates. This makes the determination of the high shear limiting viscosity difficult at higher concentrations. Thus, the viscosity data above the shear thickening transition have been removed in fitting to the Cross model. The relative zero shear viscosity and high shear

Table 2. Fitting Parameter for Modified Cross Model for 32 nm Particle Dispersion

ϕ	$\eta_{r\infty}$	η_{r0}	b	m
0.180	1.87 ± 0.03	2.82 ± 0.03	44.51 ± 0.18	1 ± 0.09
0.307	2.58 ± 0.04	6.84 ± 0.03	18.88 ± 0.80	1
0.368	3.54 ± 0.68	37.73 ± 0.81	15.30 ± 0.82	1.1 ± 0.14
0.395	7.21 ± 0.66	76.54 ± 0.12	14.5 ± 0.83	1.3 ± 0.16
0.417	11.5 ± 0.47	213.2 ± 0.83	14.04 ± 0.49	1.4 ± 0.08
0.447	54.7 ± 0.40	1033 ± 0.36	8.8 ± 0.13	1.8 ± 0.04
0.486	112.6 ± 0.59	2785 ± 8.62	10.5 ± 0.15	1.7 ± 0.03

limited viscosity from fits in Figure 6 to eq 2 are shown in Table 2. For reference, for near hard spheres Krieger[29] found $b = 2.32$ independent of the volume fraction, while de Kruif et al.[30] found that it ranged from 2.3 to 3.0, both with $m = 1$. For sterically stabilized dispersions, Mewis et al.[31] fit the shear viscosity of a colloidal dispersion of poly(methyl methacrylate) (PMMA) particles dispersed in decalin to eq 2. According to their result, the factor m increased from 1 to 3.53 at higher concentrations, but b ranged from 8.8 to 26 without monotonic tendency with variation of particle volume fraction. In our case, m shows a nearly monotonic increase with the particle volume fraction, while $b \sim 8.8-44.51$, decreasing with volume fraction.

Figure 7 shows a master plot of $(\eta_r - \eta_{r\infty})/(\eta_{r0} - \eta_{r\infty})$ against $(b\tau_r)^m$. The scaled viscosity curves for the nanoparticle dispersion are well-described by the Cross model until shear thickening. Similar plots cannot be made for 446 nm particle dispersed in EG as the low Peclet number regime is not accessible to measurement.

The zero shear viscosity at low particle concentrations can be represented by

$$\eta_r = \frac{\eta}{\eta_m} = 1 + k_1\phi + k_2\phi^2 + ... \qquad (3)$$

where $k_1 = 2.5$ and $k_2 = 2.5^2 k_H$ for spherical particles. For Brownian hard spheres, $k_2 = 5.9$.[32,33] This equation is valid for particle volume fractions lower than 0.1. Also, k_2 is very sensitive to the presence of interparticle forces. For electrostatic repulsive forces, calculations of the secondary electroviscous effect by Russel[24,34] obtained $k_2 = 2.5 + (3/40)(2a_{eff}/a)^5$, with the effective particle radius a_{eff} due to the electrostatic repulsive forces.

We compare our experimental results obtained from the rolling ball viscometer with dilute limiting predictions for the zero shear viscosity in Figure 8a. The relative viscosity exceeds predictions for hard spheres. The best fit of eq 3 to the data,

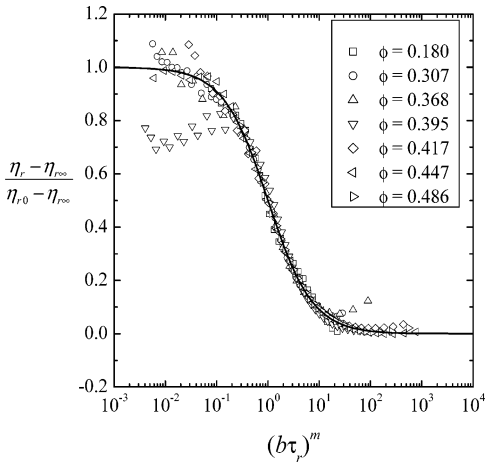

Figure 7. Master curve of the viscosity curve for 32 nm nanoparticle dispersion using reduced stress in eq 2 (solid line).

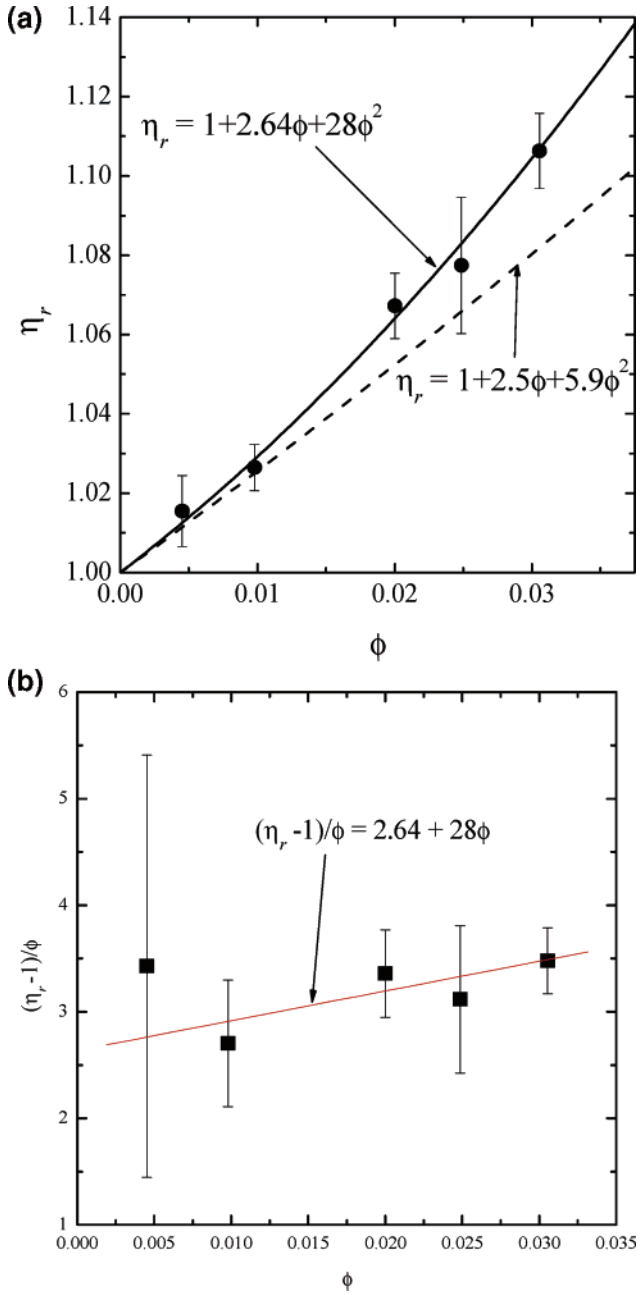

Figure 8. (a) Relative viscosity of dilute nanoparticle dispersion plotted along with the best fit (solid line) and the predictions for hard spheres (dashed line) and (b) intrinsic viscosity as function of the particle volume fraction for dilute 32 nm nanoparticle dispersions.

plotted in Figure 8b, yields $k_1 = 2.64 \pm 0.72$ and $k_H = 4.01 \pm 4.12$. This value of the Huggins coefficient corresponds to an effective hard sphere diameter of $2a_{eff} = 51$ nm. As a result of electrostatic stabilization, the effective thermodynamic radius of the nanoparticles increases beyond the hydrodynamic radius. The large increase in effective radius reflects the significant range of the electrostatic interactions for the nanoparticle dispersion; the ratio of the inverse Debye screening length to the hydrodynamic particle size (κa) for the nanoparticles is small relative to that for micrometer-size colloidal particles.

For concentrated colloidal dispersions of spherical particles, the zero shear viscosity can be fit to semiempirical relations such as the Krieger−Dougherty equation,[29]

$$\eta_{r0} = \frac{\eta_0}{\eta_m} = (1 - \phi/\phi_m)^{-k_1\phi_m} \qquad (4)$$

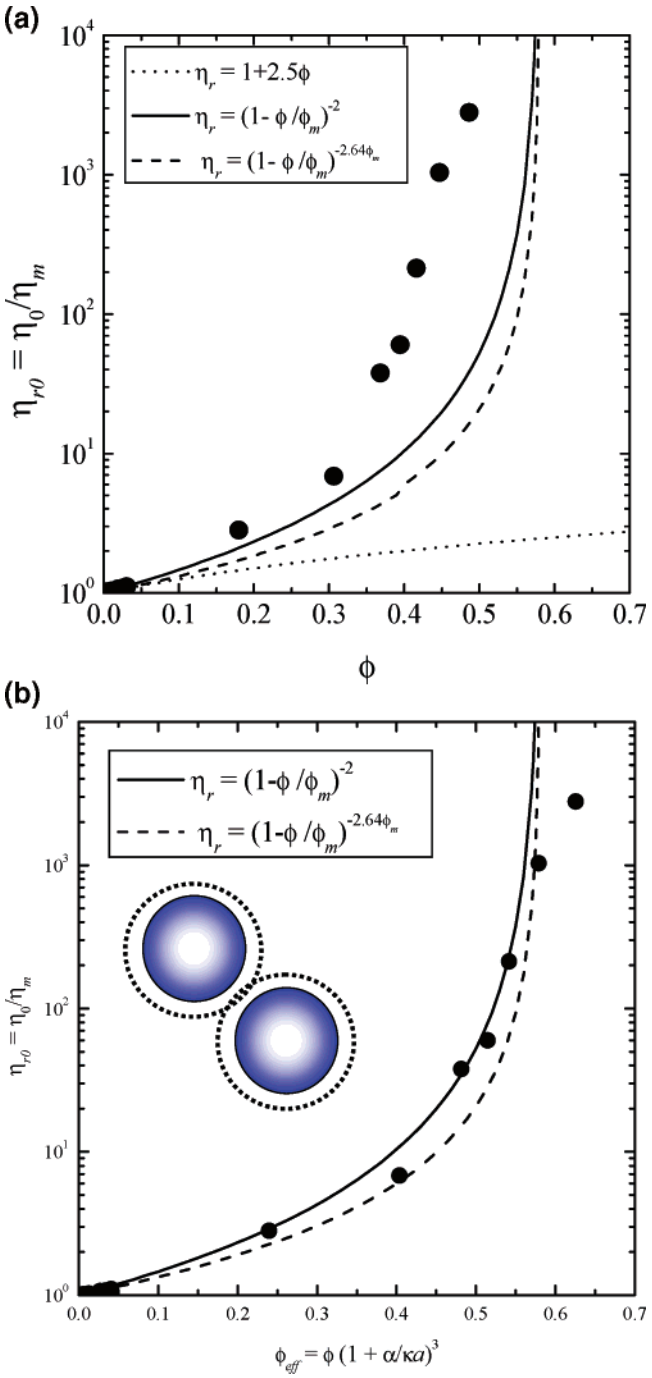

Figure 9. Relative zero shear viscosity as a function of (a) the particle volume fraction and (b) effective particle volume fraction for 32 nm nanoparticle dispersion.

or the relation[35]

$$\eta_{r0} = \frac{\eta_0}{\eta_m} = (1 - \phi/\phi_m)^{-2.0} \qquad (5)$$

where ϕ_m is the maximum packing fraction (typically on the order of 0.58−0.64 for hard spheres). Here, we use $\phi_m = 0.58$, which corresponds to the colloidal glass transition for hard spheres.

Figure 9a shows the results for the relative zero shear viscosities of the nanoparticle dispersions plotted against the hard-sphere volume fraction determined from the weight fraction and the measured densities. Clearly, the viscosity exceeds that predicted by either correlation or the Einstein equation, which indicates, not surprisingly, that the effective particle size is greater than the hydrodynamic size due to repulsive electrostatic interactions.

Table 3. Comparison of Experimental and Theoretical Critical Shear Stress for Onset of Shear Thickening for Silica Particles Dispersed in Ethylene Glycol

ϕ	κa	h_m (nm)	$\phi_{eff} = \phi(1 + a/\kappa a)^3$	predicted τ_c (Pa) with eq 8	τ_c (exp)
(a) For 32 nm Silica Particle					
0.005	5.3	4.4	0.006	1689	-
0.010	5.3	4.4	0.013	1691	-
0.020	5.3	4.4	0.027	1694	-
0.025	5.3	4.4	0.033	1696	-
0.031	5.3	4.4	0.041	1698	-
0.180	5.5	4.2	0.239	1760	-
0.307	5.7	4.1	0.404	1836	1308
0.368	5.9	4.0	0.482	1885	1349
0.395	6.0	3.9	0.514	1910	2282
0.417	6.0	3.9	0.542	1932	2303
0.447	6.1	3.8	0.579	1966	2416
0.486	6.3	3.7	0.626	2017	1882
(b) For 446 nm Silica Particle					
0.30	5.8	55.5	0.39	31	32.5
0.35	6.1	53.2	0.45	32	53.2
0.40	6.4	50.7	0.51	33	54.4
0.44	6.7	48.5	0.56	35	55.6
0.51	7.3	44.3	0.63	38	90.9
0.55	7.8	41.7	0.68	41	92.9
0.58	8.2	39.6	0.70	43	62.6

Using an approach successfully applied for similar particles,[5,36] we fit the data to eq 5 by using an effective particle

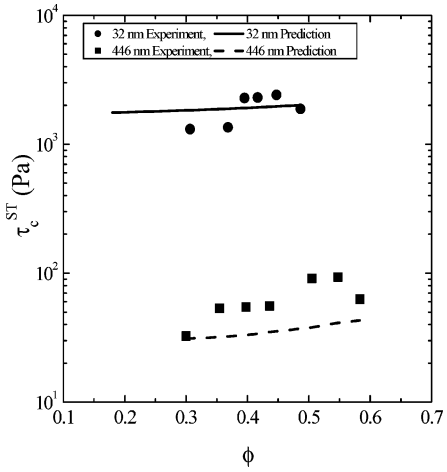

Figure 10. Critical shear stress for shear thickening as a function of volume fraction for 32 and 446 nm particle dispersions.

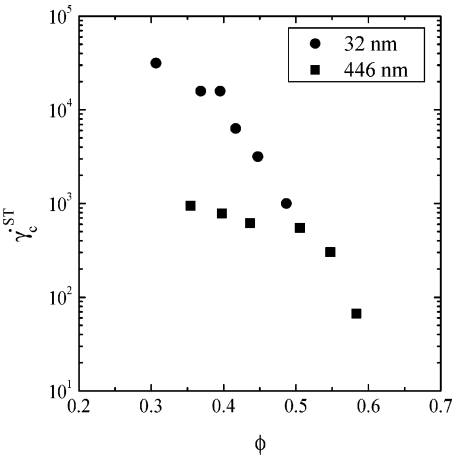

Figure 11. Critical shear rate for shear thickening as a function of volume fraction for 32 and 446 nm particle dispersions.

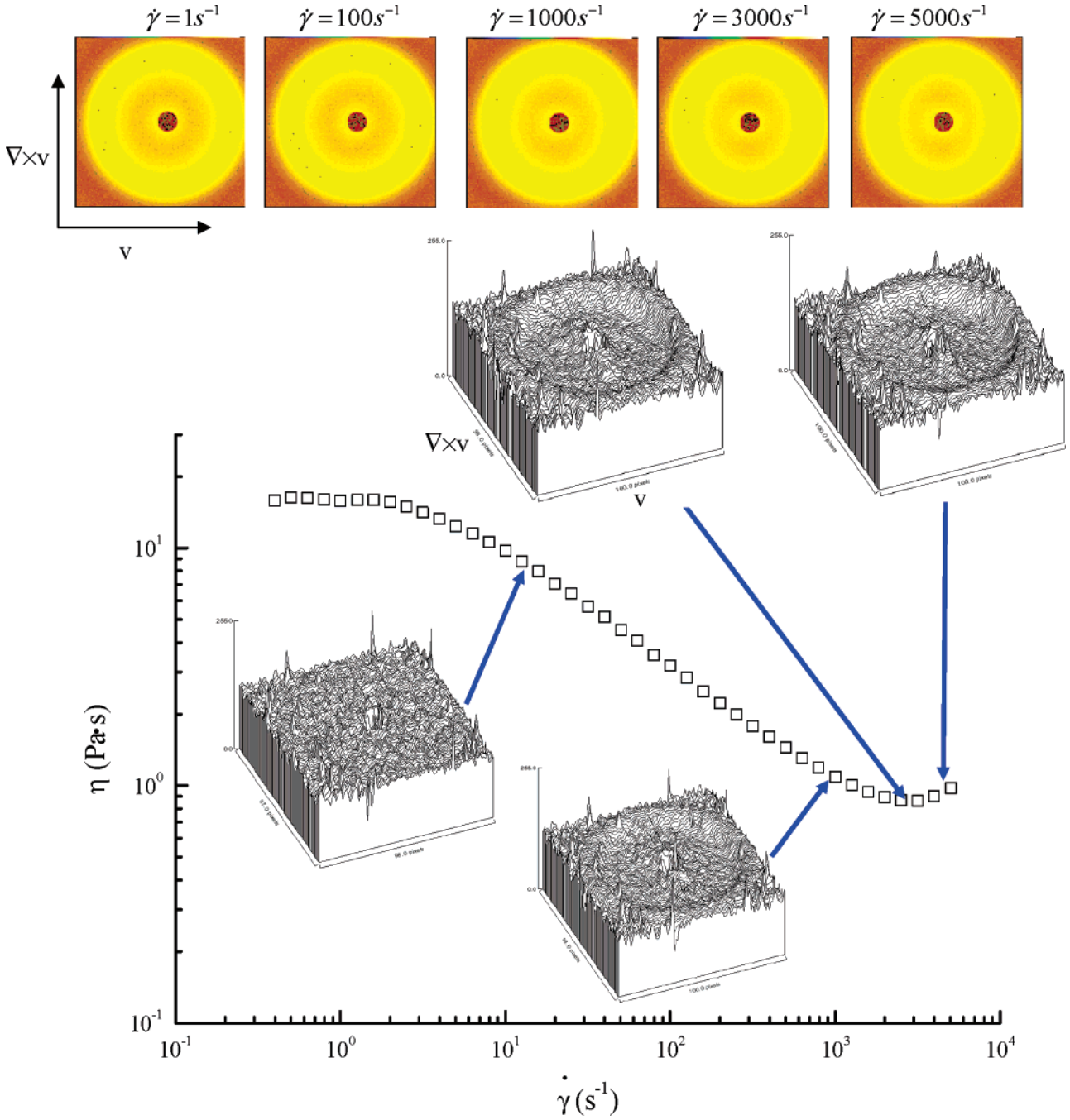

Figure 12. 2D-SANS image of the 32 nm silica dispersion ($\phi = 0.45$) at 25 °C as a function of shear rate. The 3D plots are difference spectra with the low shear rate spectra.

radius that scales with the electrostatic screening length κ^{-1} (Debye screening length) as

$$\phi_{\text{eff}} = \phi\left[1 + \frac{\alpha}{\kappa a}\right]^3 \tag{6}$$

Figure 9b shows the results of this fit with $\alpha = 0.55$ and the maximum packing fraction $\phi_m = 0.58$. The value of the coefficient α is smaller than previous results[5,36] obtained for larger, colloidal particles, showing it is not universal for all charged particle dispersions. Using the κa values reported in Table 3, this corresponds to effective particle diameters of $2a_{\text{eff}} \approx 35$ nm, which is smaller than that observed at lower volume fractions by intrinsic viscometry, as expected. At the highest volume fractions the dispersions deviate from the expected strong divergence in viscosity, which is an indication of the "softness" of the repulsive potential.

Under shear flow, hydrodynamic interactions become important and can overcome stabilizing electrostatic forces, leading to the formation of a hydroclustered microstructure.[3,9] This new microstructure leads to increased viscous dissipation and shear thickening. Using a predictive model for the onset of hydrocluster formation,[3,4,22,37] the critical shear stress can be predicted from independent measurements of the particle size, concentration, surface potential, and ionic strength. The final equation for prediction of the critical shear stress for the onset of shear thickening for dispersions stabilized by electrostatic interactions is

$$\tau_c = 0.024\frac{k_B T(\kappa a)\Psi^2}{a^2 l_b} \tag{7}$$

where l_b is the Bjerrum length defined by $l_b \equiv e^2/(4\pi\epsilon\epsilon_0 k_B T)$,

and $\Psi_s = \psi_s e/k_B T$ is the dimensionless surface potential. The experimental value of the critical stress compares well with the theoretical prediction (Table 3, Figure 10). At lower volume fractions, shear thickening is difficult to detect as the effect is small[2] and the shear rates required are difficult to achieve in the experiment. In this table h_m is the characteristic separation distance between particle surfaces in the incipient hydrocluster state, which is determined from theory as $h_m\kappa = 1.453$,[3] where κ is the inverse Debye screening length defined previously that gauges the range of the electrostatic repulsion. Molecular simulations show the characteristic intermolecular spacing for EG in the liquid state to be ~5 Å with correlations extending to ~1 nm.[38] Consequently, the interparticle spacing in the incipient hydroclusters is still larger than the molecular correlation length by a factor of 4−5 in the shear thickening state, and continuum hydrodynamics correctly describes the hydrodynamic interaction. Also shown in Figure 10 are critical stresses for the reference sample of 446 nm silica dispersions, with rheology shown in Figure 5d. The excellent agreement between the theoretical predictions and measurements support the supposition that the mechanism of shear thickening is the same in the 32 nm diameter nanoparticle dispersions as in the larger, 446 nm diameter colloidal dispersions. Apparently the relatively greater roughness of the nanoparticles does not play a significant role, probably because of the significant value of the relative electrostatic screening length (κa).

Figure 11 shows an interesting result that suggests similarities and differences remain unexplained, however, between the two systems. Figure 10 demonstrates that much higher stresses are required to induce shear thickening in the nanoparticle dispersion as compared to the colloidal dispersion, as predicted. However, Figure 11 shows that the transition *shear rates* become comparable for the two systems at volume fractions around 50%. Both systems show a decreasing critical shear rate with volume fraction, as is typical, but the nanoparticle dispersion shows a much steeper decrease at lower volume fractions. This behavior is not fully understood but may be a consequence of the more significant electrostatic double layer relative to the particle size for the nanoparticles. Also note that the relatively stronger electrostatic repulsions for the nanoparticle dispersion limit are concentrated by centrifugation to volume fractions below where *discontinuous* shear thickening is typically observed ($\phi > 0.5$). Alternatively, surface roughness may play a role in mitigating the strength of the shear thickening.[23]

B. Flow−SANS. Figure 12 shows the radial SANS pattern at various shear rates including the Newtonian plateau, shear thinning, transition to shear thickening, and shear thickening regimes for concentrated nanoparticle dispersion ($\phi = 0.45$). As shown in this figure, the continuous shear thickening transition occurs around 3000 s^{-1}. As is typical for continuously shear thickening colloidal dispersions, there are only subtle changes in the scattering pattern measured through the continuous shear thickening transition.[5,18] To identify microstructural changes, the scattering patterns at each shear rate are subtracted by the one at the lowest shear rate (here $\dot{\gamma} = 1\ s^{-1}$), which is at low enough Peclet number to represent the equilibrium state. These subtracted scattering patterns are displayed in Figure 12 as 3D plots below the original scattering patterns. Tangential patterns show an even more isotropic pattern with little change and, consequently, are not shown. Above 3000 s^{-1} of the shear rate, the distortion of the scattering patterns is most dominant in the velocity direction, as shown in Figure 12. The most significant feature of the scattering under flow is the lack of Bragg scattering,[39] which demonstrates that the shear thickening is not associated with an order−disorder transition.[40,41]

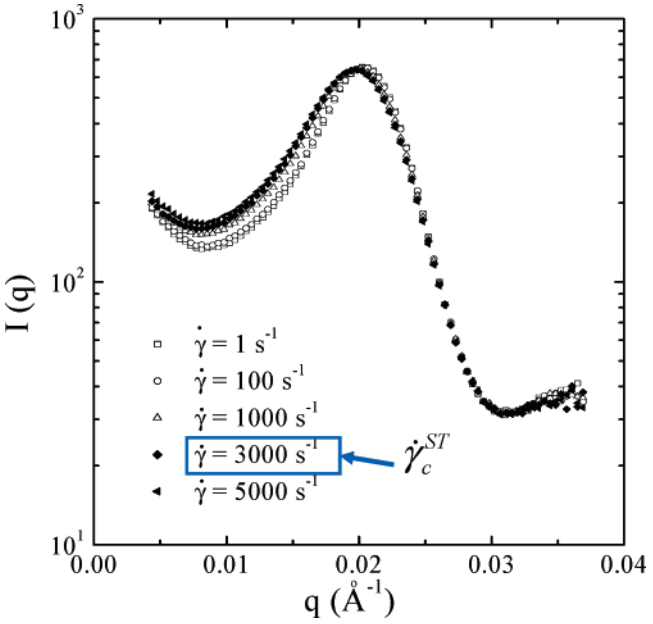

Figure 13. Plot of the circular averaged scattering intensity measured in the radial direction against the magnitude scattering vector for different shear rates.

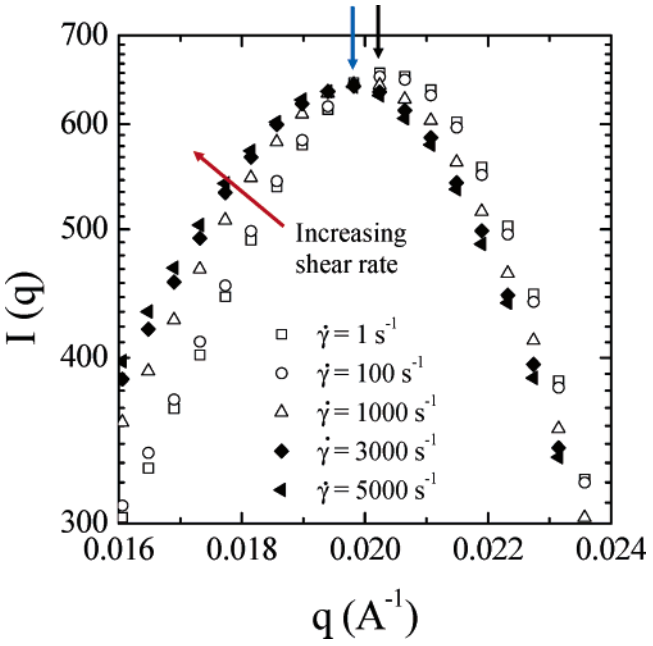

Figure 14. Peak of circular averaged scattering intensity as a function of scattering vector with different shear rates. The labels for the symbols are the same as those in Figure 13.

Figures 13 and 14 show comparison of the circularly averaged scattering intensity, $I(q)$, for the data obtained in the radial direction as a function of the scattering vector, **q**, at different shear rates. At very low shear rate ($\dot{\gamma} = 1\ s^{-1}$), which corresponds to the equilibrium state ($Pe \ll 1$), the scattering pattern shows an isotropic scattering ring due to the liquidlike spatial distribution of the nanoparticle. In the shear thinning regime ($10\ s^{-1} < \dot{\gamma} < 3000\ s^{-1}$), the peak position does not change with shear rate below 1000 s^{-1} of shear rate. Then gradual changes in the radial scattering profile have been observed with further increasing shear rate. The peak in the scattering intensity becomes broader and shifts to lower scat-

tering vector with increasing shear rate, indicating long-range correlations between the particles. This result shows only a slight redistribution of particles due to flow in both the shear thinning and shear thickening regimes; i.e., there is no order−disorder transition associated with either shear thinning or shear thickening. Rather, the result is consistent with previous SANS measurements of shear thickening dispersions that show similar structural changes, which can be quantitatively connected to the measured rheology.[5]

IV. Conclusions

Nanoparticle (32 nm) dispersions are shown to exhibit rheology that is consistent with that of colloidal dispersions at low, intermediate, and high shear rates. In particular, reversible shear thickening is evident. Also, master curves can be developed for the low shear pseudo-Newtonian plateau and shear thinning regimes similarly to those for colloidal dispersions. The volume fraction dependence of the low shear viscosity can be described by an effective particle size that depends on the electrostatic interactions between particles. Using independently determined dispersion properties, including the surface charge and associated ionic strength, theoretical predictions for the onset of shear thickening can be compared to the measured data. The results lead to the important conclusion that shear thickening in nanoparticle dispersions is consistent with the hydrocluster mechanism, which requires that continuum hydrodynamics applies to particles that are separated only by nanometers. Consequently, theoretical and experimental methods useful for studying the rheology of colloidal dispersions can be applied to nanoparticle dispersions. These conclusions are relevant for processes using nanoparticle dispersions at high shear rates, such as chemical mechanical planarization.[42]

Acknowledgment

We are pleased to contribute this work in honor of Prof. William B. Russel, who has inspired this research by providing our modern, scientific understanding of colloidal suspension rheology. N.J.W. acknowledges Prof. Russel's patient guidance and enthusiastic support through the course of his career. Dr. Leo Hanus (AZ Electronics) is acknowledged for providing the nanoparticles used in this work. This work has been supported through the Army Research Laboratory CMR program (Grant No. 33-21-3144-66) through the Center for Composite Materials of the University of Delaware. We acknowledge the support of the National Institute of Standards and Technology, U.S. Department of Commerce, in providing the neutron research facilities used in this work, and Dr. Lionel Porcar of NIST for assisting with the Rheo-SANS measurements. This work utilized facilities supported in part by the National Science Foundation under Agreement No. DME-0454672.

Literature Cited

(1) Zhao, Q. Q.; Boxman, A.; Chowdhry, U. Nanotechnology in the chemical industry−Opportunities and challenges. *J. Nanopart. Res.* **2003**, *5*, 567−572.

(2) Bergenholtz, J.; Brady, J. F.; Vicic, M. The non-Newtonian rheology of dilute colloidal suspensions. *J. Fluid Mech.* **2002**, *456*, 239−275.

(3) Maranzano, B. J.; Wagner, N. J. The effect of interparticle interactions and particle size on reverse shear thickening: Hard-sphere colloidal dispersions. *J. Rheol. (N. Y.)* **2001**, *45*, 1205−1222.

(4) Maranzano, B. J.; Wagner, N. J. The effect of particle size on reverse shear thickening of concentrated colloidal dispersion. *J. Chem. Phys.* **2001**, *114*, 10514−10527.

(5) Maranzano, B. J.; Wagner, N. J. Flow-small angle neutron scattering measurements of colloidal dispersion microstructure evolution through the shear thickening transition. *J. Chem. Phys.* **2002**, *117*, 10291−10302.

(6) Laun, H. M.; Bung, R.; Hess, S.; Loose, W.; Hess, O.; Hahn, K.; Hadicke, E.; Hingmann, R.; Schmidt, F.; Lindner, P. Rheological and small angle neutron scattering investigation of shear-induced particle structures of concentrated polymer dispersions submitted to plane Poiseuille and Couette flow. *J. Rheol. (N. Y.)* **1992**, *36*, 743−787.

(7) Bossis, G.; Brady, J. F. The rheology of Brownian suspensions. *J. Chem. Phys.* **1989**, *91*, 1866−1874.

(8) Catherall, A. A.; Melrose, J. R.; Ball, R. C. Shear thickening and order−disorder effects in concentrated colloids at high shear rates. *J. Rheol. (N. Y.)* **2000**, *44*, 1−25.

(9) Bender, J. W.; Wagner, N. J. Reversible shear thickening in monodisperse and bidisperse colloidal dispersions. *J. Rheol. (N. Y.)* **1996**, *40*, 899−916.

(10) Bender, J. W.; Wagner, N. J. Optical measurement of the contributions of colloidal forces to the rheology of concentrated suspension. *J. Colloid Interface Sci.* **1995**, *172*, 171−184.

(11) Lee, Y. S.; Wagner, N. J. Dynamic properties of shear thickening colloidal suspensions. *Rheol. Acta* **2003**, *42*, 199−208.

(12) Helber, R.; Doncker, F.; Bung, R. Vibration attenuation by passive stiffness switching mounts. *J. Sound Vib.* **1990**, *138*, 47−57.

(13) Laun, H. M.; Bung, R.; Schmidt, F. Rheology of extremely shear thickening polymer dispersions (passively viscosity switching fluids). *J. Rheol. (N. Y.)* **1991**, *35*, 999−1034.

(14) Shenoy, S. S.; Wagner, N. J.; Bender, J. W. E.-FiRST: Electric field responsive shear thickening fluids. *Rheol. Acta* **2003**, *43*, 287−294.

(15) Lee, Y. S.; Wetzel, E. D.; E. G. E., Jr.; Wagner, N. J. In Advanced Body Armor Utilizing Shear Thickening Fluids. *Proceedings of 23rd Army Science Conference*, Orlando, FL, Dec. 2−5, 2002; Assistant Secretary of the Army (Acquisition, Logistics and Technology): Arlington, VA; pp A0−01.

(16) Lee, Y. S.; Wetzel, E. D.; Wagner, N. J. The ballistic impact characteristics of Kevlar woven fabrics impregnated with a colloidal shear thickening fluid. *J. Mater. Sci.* **2003**, *38*, 2825−2833.

(17) D'Haene, P. D.; Mewis, J.; Fuller, G. G. Scattering dichroism measurements of flow-induced structure of a shear thickening suspension. *J. Colloid Interface Sci.* **1993**, *156*, 350−358.

(18) Newstein, M. C.; Wang, H.; Balsara, N. P.; Lefebvre, A. A.; Shnidman, Y.; Watanabe, H.; Osaki, K.; Shikata, T.; Niwa, H.; Morishima, Y. Microstructural changes in a colloidal liquid in the shear thinning and shear thickening regimes. *J. Chem. Phys.* **1999**, *111*, 4827−4838.

(19) Watanabe, H.; Yao, M.-L.; Osaki, K.; Shikata, T.; Hirokazu, N.; Morishima, Y.; Balsara, N. P.; Wang, H. Nonlinear rheology and flow-induced structure in a concentrated spherical silica suspension. *Rheol. Acta* **1998**, *37*, 1−6.

(20) Melrose, J. R.; Viliet, J. H.; Ball, R. C. Continuous shear thickening and colloid surfaces. *Phys. Rev. Lett.* **1996**, *77*, 4660−4663.

(21) Wagner, N. J.; Bender, J. W. The role of nanoscale forces in colloid dispersion rheology. *MRS Bull.* **2004**, 100−106.

(22) Krishnamurthy, L.; Wagner, N. J.; Mewis, J. Shear thickening in polymer stabilized colloidal dispersions. *J. Rheol. (N. Y.)* **2005**, *49*, 1347−1360.

(23) Lootens, D.; van Damme, H.; Hemar, Y.; Hebraud, P. Dilatant flow of concentrated suspensions of rough particles. *Phys. Rev. Lett.* **2005**, *95*, 268302.

(24) Russel, W. B. Review of the role of colloidal forces in the rheology of suspensions. *J. Rheol. (N. Y.)* **1980**, *24*, 287−317.

(25) Russel, W. B.; Saville, D. A.; Schowalter, W. R. *Colloidal Dispersion*; Cambridge University Press: Cambridge, U.K., 1989.

(26) Reiter, G.; Demirel, A. L.; Granick, S. From static to kinetic friction in confined liquid films. *Science* **1994**, *266*, 1741−1744.

(27) Mackay, M. E.; Dao, T. T.; Tuteja, A.; Ho, D. L.; Horn, B. V.; Kim, H.-C.; Hawker, C. J. Nanoscale effects leading to non-Einstein-like decrease in viscosity. *Nat. Mater.* **2003**, *2*, 762−766.

(28) Porcar, L.; Hamilton, W. A.; Butler, P. D.; Waar, G. G. A vapor barrier Couette shear cell for small angle neutron scattering measurements. *Rev. Sci. Instrum.* **2002**, *73*, 2345−2354.

(29) Krieger, I. M. Rheology of monodisperse lattices. *Adv. Colloid Interface Sci.* **1972**, *3*, 111−136.

(30) de Kruif, C. G.; van lersel, E. M. F.; Vrij, A.; Russel, W. B. Hard sphere colloidal dispersions: Viscosity as a function of shear rate and volume fraction. *J. Chem. Phys.* **1985**, *83*, 4717−4725.

(31) Mewis, J.; Frith, W. J.; Strivens, T. A.; Russel, W. B. The rheology of suspensions containing polymerically stabilized particles. *AIChE J.* **1989**, *35*, 415−422.

(32) Batchelor, G. K. Effect of Brownian-motion on bulk stress in a suspension of spherical-particles. *J. Fluid Mech.* **1977**, *83*, 97−117.

(33) Bergenholtz, J.; Wagner, N. J. The Huggins coefficient for the square-well fluid. *Ind. Eng. Chem. Res.* **1994**, *33*, 2391−2403.

(34) Russel, W. B. Bulk stresses due to deformation of electrical double-layer around a charged sphere. *J. Fluid Mech.* **1978**, *85*, 673−683.

(35) Quemada, D. Rheology of concentrated disperse systems and minimum energy dissipation principle. I. Viscosity-concentration relationship. *Rheol. Acta* **1977**, *16*, 82−94.

(36) Wagner, N. J.; Krause, R.; Rennie, A. R.; D'Aguanno, B.; Goodwin, J. The microstructure of polydisperse, charged colloidal suspensions by light and neutron scattering. *J. Chem. Phys.* **1991**, *95*, 494−508.

(37) Shenoy, S. S.; Wagner, N. J. Influence of medium viscosity and adsorbed polymer on the reversible shear thickening transition in concentrated colloidal dispersions. *Rheol. Acta* **2005**, *44*, 360−371.

(38) Saiz, L.; Padro, J. A.; Guardia, E. Structure of liquid ethylene glycol: A molecular dynamics simulation study with different force fields. *J. Chem. Phys.* **2001**, *114*, 3187−3199.

(39) Butera, R. J.; Wolfe, M. S.; Bender, J. W.; Wagner, N. J. Formation of a highly ordered colloidal microstructure upon flow cessation from high shear rates. *Phys. Rev. Lett.* **1996**, *77*, 2117−2120.

(40) Hoffman, R. L. Discontinuous and dilatant viscosity behavior in concentrated suspensions. II. Theory and experimental tests. *J. Colloid Interface Sci.* **1974**, *46*, 491−506.

(41) Hoffman, R. L. Explanations for the cause of shear thickening in concentrated colloidal suspensions. *J. Rheol. (N. Y.)* **1997**, *42*, 111−123.

(42) Li, Z.; Ina, K.; Lefevre, P.; Koshiyama, I.; Philipossian, A. Determining the effects of slurry surfactant, abrasive size, and abrasive content on the tribology and kinetics of copper CMP. *J. Electrochem. Soc.* **2005**, *152* (4), G299−G304.

Received for review November 16, 2005
Revised manuscript received May 20, 2006
Accepted May 25, 2006

IE0512690